

Understanding tunneling ionization of atoms in laser fields with the essence of multiphoton absorption*

Long Xu and Li-Bin Fu[†]

*Graduate School of China Academy of Engineering Physics,
No. 10 Xibeiwang East Road, Haidian District, Beijing, 100193, China*

The elaborate energy and momentum spectra of ionized electrons from atoms in laser fields suggest that the ionization dynamics described by tunneling theory should be modified. Although many efforts have been done within semiclassical models, there are few discussions describing multiphoton absorption process with quantum framework. In this letter, by comparing the results obtained with the time-dependent Schrödinger equation (TDSE) and Keldysh-Faisal-Reiss (KFR) theory, we have studied the nonperturbative effects of ionization dynamics beyond KFR theory. The difference in momentum spectra between multiphoton and tunneling regimes is understood in a unified picture with virtual multiphoton absorption processes. For the multiphoton regime, the momentum spectra can be obtained by coherent interference of each periodic contribution. However, the interference of multiphoton absorption peaks will result in the complex structure of virtual multiphoton bands in the tunneling regime. It is shown that the virtual spectra will be almost continuous in the tunneling regime instead of the discrete levels in the multiphoton regime. Finally, with a model combining TDSE and KFR theory, we have tried to understand the different effects of virtual multiphoton processes on ionization dynamics.

PACS numbers: 32.80.-t, 32.80.Rm, 42.50.Ct

The behavior of electron in a strong laser field has attracted considerable interest, especially after the observation of above-threshold ionization (ATI) [1], where the electron can absorb more photons than that required to overcome the ionization potential. Since then, a variety of experiments have been performed in order to reveal the underlying mechanisms of various phenomena appeared in the strong field, such as the ATI [2–5], tunneling ionization [6–9], and high-order harmonic generation (HHG) [10–12].

The interaction of atoms with strong laser fields can be studied numerically with TDSE [13–16], classical [17, 18] or semiclassical approaches [19–21]. By using semiclassical methods, we can understand the profound physical processes and come to universal results. Here, most of the semiclassical methods are based on the KFR theory [22–25], which can result in qualitative agreement with the results of exact TDSE or experiments, e.g. the energy spectra of ATI [26, 27]. KFR theory ignores the dynamics of the bound states and the coulomb effect on the continuum states. In the past, many efforts have been made in the KFR theory’s amendments, which mainly considers the Coulomb interaction, such as Coulomb-Volkov approximation [28–30] and the rescattering models of Strong Field Approximation [31]. The effects of the excited states [32, 33] and the depletion effect of the ground state [4, 34] have also been evaluated within the KFR theory.

In the pioneering paper of KFR theory, Keldysh first

proposed the so-called Keldysh parameter [22] defined as $\gamma \equiv \sqrt{I_P/2U_P}$, where I_P is the ionization potential and $U_P = E_0^2/4\omega^2$ is the ponderomotive energy. Here E_0 and ω are the amplitude and frequency of laser pulse, respectively. The asymptotic behavior of the ionization rate at $\gamma \rightarrow 0$ tends to the case of electron tunneling in a static field [35]. Hence when $\gamma \ll 1$, the ionization process is known as the tunneling regime, whereas it is regarded as the multiphoton regime for $\gamma \gg 1$ [36, 37], although both of their processes are related to multiphoton absorption. It’s widely accepted that KFR theory only works in the tunneling regime. Besides, both the semiclassical methods [19–21] and the rescattering models of Strong Field Approximation [31] work very well in the tunneling regime where the rescattering effect dominates the dynamics.

Most recently, considerable amount of attention are paid to ionization dynamics in the crossover regime ($\gamma \sim 1$), where nonadiabatic effects [38–40] and modifications of the semiclassical methods [41, 42] have been discussed. These discussions are triggered by the fact that the momentum spectra observed in the experiments indicate that the tunneling ionization theory should be modified. Many efforts combining multiphoton and tunneling processes have also been made to understand the ionization process in the tunneling and crossover regimes [33, 43]. In these regimes, the rescattering effect dominates the dynamics and covers the other nonperturbative effects. Hence, to investigate the modifications of ionization dynamics beyond KFR theory, we need a unified model that excludes rescattering process to bridge the multiphoton and tunneling regimes.

In this letter, by solving TDSE and comparing the results with KFR theory, we find the virtual multiphoton absorption processes play an important role in under-

* Supported by National Natural Science Foundation of China (No. 11725417, 11575027), NSAF (Grant No. U1730449), and Science Challenge Project (Grant No. TZ2018005).

[†] Corresponding author. Email: lbfu@gscaep.ac.cn

standing multiphoton and tunneling ionization dynamics in a unified picture. Then, with a model that combines TDSE and KFR theory, we investigate the nonperturbative effects of ionization dynamics other than the rescattering effect. Based on such a model, we illustrate different nonperturbative effects by filtering the contribution of the virtual multiphoton process and understand them essentially from the multiphoton absorption.

Without loss of generality, we consider a one dimensional model (in atomic units):

$$i\frac{\partial}{\partial t}\Phi(x,t) = \left[-\frac{1}{2}\frac{\partial^2}{\partial x^2} - \frac{1}{\sqrt{x^2+a^2}} + xE(t) \right] \Phi(x,t), \quad (1)$$

where the second and third terms in the right hand represent the soft-core electron-nucleus interaction and the atom-field interaction, respectively. The soft-core parameter is chosen as $a^2 = 0.484$ in order to reproduce singly charged helium atom. The pulse is designed as $E(t) = -\partial A(t)/\partial t$ with the vector potential $A(t) = E_0/\omega \sin^2(\pi t/\tau) \cos(\omega t)$, with τ as the pulse duration. In the simulation, a total of 16 optical cycles are used unless stated otherwise. In the numerical calculations, we employ the split-operator method [44] to solve TDSE and imaginary-time propagation to compute the singlet ground state as the initial wave function.

Furthermore, we can expand the unknown wave function in terms of the basis combining the bound wave function $\varphi_n(x,t)$ and Volkov function $\psi_p(x,t) = (2\pi)^{-1/2} \exp\{i[p + A(t)]x - i\int_0^t [p + A(t')]^2/2dt'\}$ as

$$\Phi(x,t) = \sum_p a_p(t)\psi_p(x,t) + \sum_n b_n(t)\varphi_n(x,t). \quad (2)$$

Then, substituting the expansion (2) into the Schrödinger equation (1) and making assumptions: (a) Coulomb interaction is neglected for continuum states; (b) the population of all the excited states is ignored, we have

$$i\frac{\partial}{\partial t}a_p(t) = b_g(t)\langle\psi_p(x,t)|xE(t)|\varphi_g(x,t)\rangle, \quad (3)$$

$$i\frac{\partial}{\partial t}b_g(t) = -\sum_p a_p(t)\langle\varphi_g(x,t)|\frac{1}{\sqrt{x^2+a^2}}|\psi_p(x,t)\rangle. \quad (4)$$

Moreover, after making the assumption (c): the dynamics of ground state is neglected, we will obtain the final ionization amplitude, which retains the original choice of Keldysh [22],

$$i\frac{\partial}{\partial t}a_p(t) = \langle\psi_p(x,t)|xE(t)|\varphi_g(x,t)\rangle. \quad (5)$$

Keldysh arrived at the ionization rate by integrating the momentum distribution (see Eq. (5)). After using Fourier series expanding the expression and using the saddle-point method calculating the integration, the probability of direct ionization from the ground state was obtained, where factor γ was introduced [22]. KFR theory can describe the ionization rate well, but it fails to predict the structures of energy distribution, that is, the

positions of energy peaks are completely different from the results of TDSE when γ is small (see Figs. 1(a) and 1(b)). Rescattering events mainly affect the yield of high-energy photoelectrons (energy is greater than $2U_P$). Besides the rescattering effect, there are still other nonperturbative effects which lead KFR theory to deviate from the actual results for small γ .

To gain the physical insights over the Keldysh parameter, we will study the exact ionization dynamics with different γ . Firstly, we calculate the integrand of Eq. (5) and plot the square of its module, namely, $|\langle\psi_p(x,t)|xE(t)|\varphi_g(x,t)\rangle|^2$, in Fig. 1(c). At a given moment, $|\langle\psi_p(x,t)|xE(t)|\varphi_g(x,t)\rangle|^2$ as a function of momentum shows a bimodal structure, which does not change with the time and its center position moves with $A(t)$ between $-A_0$ and A_0 , that is, the variation of offset caused by laser field is $2A_0 = 4\sqrt{U_P}$. Additionally, we scan the ionization potential by choosing different soft-core parameters and plot the distance between two peaks of the bimodal structure as a function of $\sqrt{I_P}$ in Fig. 1(d), where the distance equals $1.61\sqrt{I_P} + 0.294$. Fig. 2 shows the momentum distributions of one and 16 optical cycles. For the energy spectra of one cycle, both the results of TDSE and KFR theory show similar results with bimodal structures at $\gamma = 8$ and arched structures at $\gamma = 0.5$. The momentum spectrum of one cycle is a bimodal structure for large γ . And when the offset variation $4\sqrt{U_P}$ of the center position of $|\langle\psi_p(x,t)|xE(t)|\varphi_g(x,t)\rangle|^2$ is greater than the distance $1.61\sqrt{I_P} + 0.294$ between the two peaks of $|\langle\psi_p(x,t)|xE(t)|\varphi_g(x,t)\rangle|^2$, namely, $\gamma < 1.76$, the mo-

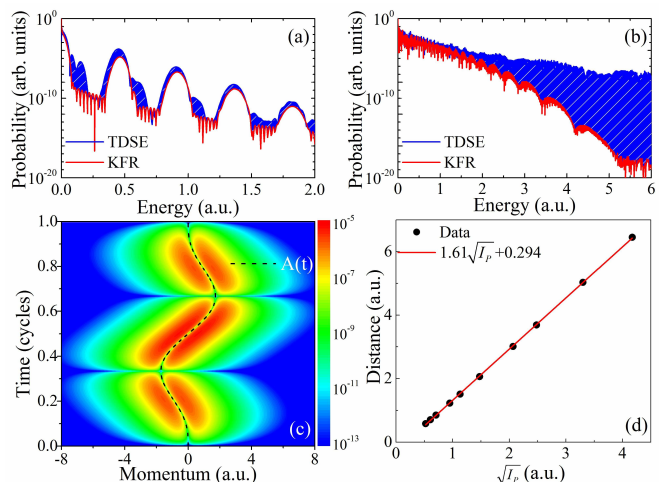


FIG. 1. Normalized energy distributions calculated by TDSE (blue) and KFR theory (red) for the wavelength are (a) 100 nm (Keldysh parameter $\gamma = 8$), (b) 1600 nm (Keldysh parameter $\gamma = 0.5$), respectively, with the laser intensity is $2 \times 10^{14} \text{ W/cm}^2$, where blue shading areas represent the difference between TDSE and KFR theory calculations. (c) $|\langle\psi_p(x,t)|xE(t)|\varphi_g(x,t)\rangle|^2$ as a function of momentum and time for the case of (b), where the dashed line represents the vector potential $A(t)$. (d) The distance between two peaks of $|\langle\psi_p(x,t)|\varphi_g(x,t)\rangle|^2$ is plotted as a function of $\sqrt{I_P}$, i.e., the 0.5th power of ionization potential.

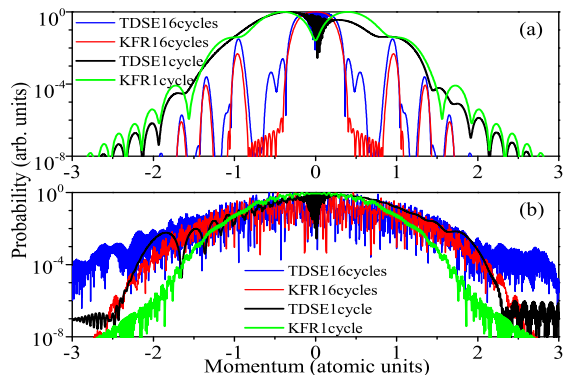


FIG. 2. Normalized momentum distributions for the cases shown in Figs. 1(a) and 1(b). Blue and black lines represent the results of TDSE for 16 optical cycles (blue) and one cycle (black), while red and green lines denote the results of KFR theory for 16 cycles (red) and one cycle (green), respectively.

mentum distribution of one cycle will be merged into an arched structure. Clearly, the two extreme cases are consistent with the usual classification using the Keldysh parameter: the tunneling regime at $\gamma \ll 1$ and the multiphoton regime at $\gamma \gg 1$.

Figure 2(a) shows that the results of 16 cycles calculated by TDSE and KFR theory in the multiphoton regime are similar (also can be seen in Fig. 1(a)), and their envelopes can be described by the results of one cycle, and these are consistent in TDSE and KFR. In the tunneling regime, the momentum distribution of KFR theory runs away from TDSE. Comparing with the clear ATI peaks in the multiphoton regime, the energy spectrum in the tunneling regime is more complicated although both of them are multiphoton absorption. The blue shading areas in Fig. 1 show the difference between the results of TDSE and KFR theory, and the difference results from the dynamics of all the bound states and the coulomb effect on the continuum states. The rescattering takes over the behavior of high-energy spectrum for $\gamma \ll 1$, which has been studied essentially [31]. In addition to the rescattering effect, however, there should be other nonperturbative effects, which are not included in the KFR theory and semiclassical models [19–21], also contribute to the blue shading areas.

Besides the rescattering, the evolution of the ground-state has also been ignored in the KFR theory and it should contain important information about dynamics. Here, we apply Fourier Transform $F(E_0, \omega, \Omega) = (2\pi)^{-1} \int c_g(E_0, \omega, t) e^{-i\Omega t} dt$ to extract the information carried by the ground-state population $c_g(E_0, \omega, t) = |\langle \varphi_g(x, t) | \Phi(x, t) \rangle|^2$, where Ω is the frequency of Fourier spectra. The results of frequency spectrum analysis are plotted in Fig. 3. Figs. 3(a) and 3(b) show significantly enhanced probability in the region of Ω between 0.5 and 1 a.u. and this is related to the excited states and details will be shown in Fig. 4. Additionally, there are always even laser frequencies in the spectra (also can be seen in Fig. 4), which are the behaviors of virtual multiphoton

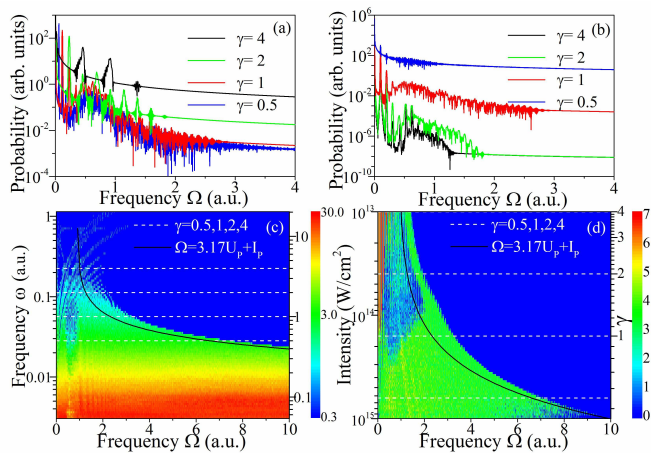


FIG. 3. Frequency spectrum analysis of the ground-state population for different Keldysh parameters. (a) The laser intensity is fixed as $2 \times 10^{14} \text{ W/cm}^2$, and the number of oscillations is plotted in (c). (b) The laser frequency is kept as 0.05 a.u., and the number of oscillations is plotted in (d). The solid lines in (c) and (d) guide the structures of the maximum of frequency Ω as a function of Keldysh parameter.

processes. According to Floquet’s theory [45], there are Floquet states by emitting or absorbing integer photons from bound states in the presence of periodic laser field and the wave function changes parity after absorbing or emitting a photon as seen from dipole matrix element. Judging from the form of the ground-state population, we know that only the states whose parity is the same as the ground state will show in the ground-state population. With decreasing γ , the peaks of virtual multiphoton absorption are broadening and interfering with each other, resulting in the Fourier spectra become incoherent and chaotic. These features can be found clearly in Figs. 3(c) and 3(d) where we count the numbers of peaks of Fourier spectra and plot the numbers as a function of γ . Clearly, the range of oscillation can be depicted as $\Omega = 3.17U_p + I_p$, which agrees with the cutoff of HHG [3, 34], shows that the maximum energy of the electron returns to the ground state is $3.17U_p$ as well.

The above Fourier spectra show that the incoherent and chaotic structures resulting from the interference between virtual multiphoton absorption peaks. Additionally, the energy of interaction is $d \cdot E(t)$, where d is the dipole moment, and the separation of adjacent peaks is photon frequency ω . At the region $d \cdot E_0 \gg \omega$ ($\gamma \ll 1$), the peaks interfere with each other. In other words, if laser intensity is kept constant and ω becomes smaller, the increasing Floquet states make the separation to be smaller. If ω is kept constant and the laser intensity becomes higher, namely, the energy of interaction is larger, the more states will be coupled. Consequently, owing to the more states are involved in the dynamics, the interference between virtual multiphoton processes will be incoherent, leading to the chaos of spectrum.

We know that the real chaotic structure is caused by incommensurate frequencies are involved. To show this

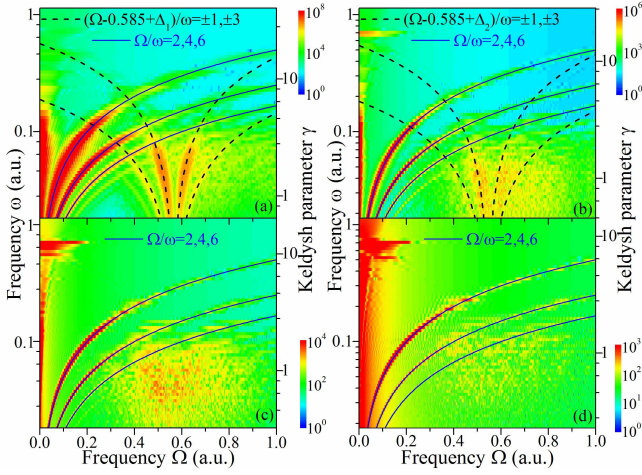


FIG. 4. Fourier spectra of ground-state population with the laser frequency is scanned from 0.02 to 1.1 a.u. for different intensities: (a) 0.5, (b) 1, (c) 2, (d) $4 \times 10^{14} \text{W/cm}^2$, respectively. Normalized by the corresponding final probability $F(E_0, \omega, \Omega = \infty)$. Blue solid lines represent the frequency of Fourier spectra that satisfies $\Omega/\omega = 2, 4, 6$, while black dashed lines guide the structures of virtual photons correlated with the first excited state in (a) and (b).

clearly, we discuss the features of the region near the first excited state, $\Omega = 0.585 a.u.$ [44]. We obtain the ground-state population by scanning the laser frequency for four different laser intensities and plot the Fourier spectra of the population in Fig. 4, which are normalized by $F(E_0, \omega, \Omega = \infty)$. In Fig. 4, we use $\Omega/\omega = 2, 4, 6$ and $(\Omega - 0.585)/\omega = \pm 1, \pm 3$ to mark the two groups of data, where 2, 4, 6 and $\pm 1, \pm 3$ are due to the parity. Fig. 3 shows that even laser frequencies come from the Floquet states related to the ground state and the features of the region near $\Omega = 0.585 a.u.$ result from the contribution of the Floquet states correlated with the first excited state. We know that one of the AC Stark shift is proportional to αE_0^2 [46], where α represents the static polarizability of an atom, so we choose $\Delta_1 = 0.02 a.u.$ and $\Delta_2 = 0.04 a.u.$ in order to match the structures. Additionally, with increasing laser intensity, these features become more complex and chaotic for quite a strong field, which are attributed to the coupling of more incommensurate frequencies.

From the above discussions, we combine multiphoton and tunneling ionization behaviors by coming up with a unified picture with virtual multiphoton absorption, as shown in Fig. 5. Fig. 5 presents the diagrammatic sketch of transition between various energy levels for different Keldysh parameters. When γ is large, even laser frequencies are always present in the frequency spectra (see Figs. 3 and 4), indicating that electron can jump between the ground state and Floquet states related by virtual multiphoton absorption. Owing to the spectral line width of the laser pulse, there are discrete bands of energy under the threshold, instead of energy levels (see Fig. 5(a)). On the contrary, when γ is small, the fre-

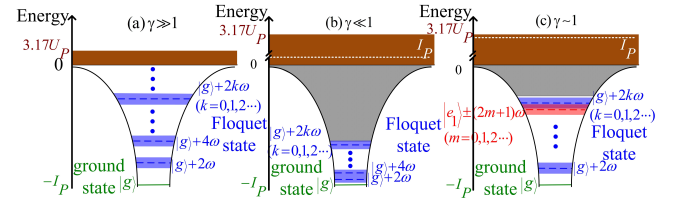


FIG. 5. Partial diagrammatic sketch of transition between various energy levels for different Keldysh parameters. Green, gray and brown lines represent the ground state, intermediate virtual states, and continuum states, while blue and red lines represent Floquet states correlated with the ground and first excited state, respectively. Red lines can also represent the effect of highly excited states. The shadow represents the effect of the spectral bandwidth and only the state whose parity is the same as the ground state is plotted in the figure.

quency spectra will be chaotic, as shown in Figs. 3(c) and 3(d), illustrating that the whole states will be connected together into a single stretch (see Fig. 5(b)). In Fig. 5(b), the gray area represents the intermediate virtual states formed by coupling the continuum states with the laser field, and the lowest energy is determined by the laser strength E_0 . Under the level of lowest energy, the Floquet states associated with ground state link up into a single stretch as well, mainly due to the interference of virtual multiphoton absorption peaks. Finally, the behavior of electron appears as tunneling from the ground state. For the crossover regime ($\gamma \sim 1$), as presented in Fig. 5(c), there are still discrete energy bands under the lowest energy and correspondingly, the behavior of electron is shown as tunneling from a virtual excited state or real excited state in the semiclassical image.

Furthermore, it is meaningful to investigate the performance of different virtual band structures on the energy spectrum. Substituting the ground-state population calculated by TDSE into Eq. (3), we have

$$i \frac{\partial}{\partial t} a_p(t) = \sqrt{c_g(t)} \langle \psi_p(x, t) | x E(t) | \varphi_g(x, t) \rangle. \quad (6)$$

To investigate the contribution of different virtual bands, we apply the Fourier transform to $c_g(t)$ and obtain the new population $c'_g(t)$ by performing the inverse Fourier transform on the filtered spectrum. In other words, the new population with filtering can be obtained by $c'_g(t) = |(2\pi)^{-1} \int \int c_g(t) e^{-i\Omega t} dt f^K(\Omega) e^{i\Omega t} d\Omega|$, where $f^K(\Omega) = 1$ (if $|\Omega| \leq \Omega^K$) or 0 (otherwise) is the filtering function with the filtering frequency Ω^K . We use $f^K(\Omega)$ with different smoothing decay and the results are qualitatively consistent. The results of the model with different filtering frequencies are plotted in Fig. 6, in which we filter the frequencies of the population $c_g(t)$ for three cases.

Apparently, the result of TDSE is fairly different from others because it contains all the information about dynamics and the rescattering effect covers the other effects. Besides, the result of the model with $\Omega^K = 3\omega$ is the same as the KFR theory, while the other filtering results are similar to KFR theory only in the region of energy lower

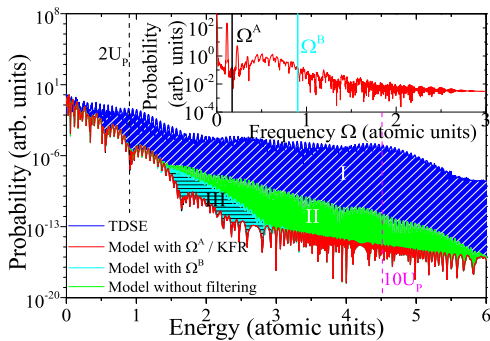


FIG. 6. Energy distributions calculated by TDSE, KFR theory and the model with different filtering frequencies. The laser frequency and intensity are 800 nm, $2 \times 10^{14} \text{W/cm}^2$, respectively. The results of the KFR theory and the model with $\Omega^A = 3\omega$ are completely coincident, while cyan (Model with $\Omega^B = I_P$) and green (Model without filtering) lines are the same as the red line for energy lower than $2U_P$. The frequency spectrum is plotted in the inset.

than $2U_P$. Comparing with the result of KFR theory, the filtering results are several orders of magnitude higher for energy greater than $2U_P$. Here the energy distribution with $\Omega^K = I_P$ only affects a small region and energy of region improved by the result without filtering is even up

to $10U_P$. As shown in Fig. 6, the energy distribution is divided into three parts, where region I represents the behavior of rescattering, while regions II and III represent the nonperturbative effects of chaotic virtual multiphoton bands and excited states, respectively.

In summary, we find that, even with the rescattering process ignored, the momentum spectra for both the multiphoton and tunneling regimes are still quite different. Such difference is caused by the nonperturbative effects of ionization dynamics beyond KFR theory, such as the dynamics of the ground state. In the multiphoton regime, the momentum spectra of many cycles can be obtained by coherent interference of contributions from each cycle. However, during the interference of intercycle, the breadths of multiphoton absorption peak will result in the complex structure in the tunneling regime. Moreover, the virtual spectra are almost continuous in the tunneling regime instead of the discrete bands in the multiphoton regime. The virtual multiphoton absorption processes play an important role in understanding multiphoton and tunneling ionization dynamics. Finally, we put forward a model to understand the different effects of virtual multiphoton processes on the ionization dynamics.

-
- [1] Agostini P et al 1979 *Phys. Rev. Lett.* **42** 1127
[2] Freeman R R et al 1987 *Phys. Rev. Lett.* **59** 1092
[3] Schafer K J et al 1993 *Phys. Rev. Lett.* **70** 1599
[4] Milošević D B et al 2010 *J. Phys. B* **43** 015401
[5] Gong X et al 2015 *Phys. Rev. Lett.* **114** 163001
[6] Augst S et al 1989 *Phys. Rev. Lett.* **63** 2212
[7] Urbain X et al 2004 *Phys. Rev. Lett.* **92** 163004
[8] Wu J et al 2012 *Phys. Rev. Lett.* **108** 183001
[9] Camus N et al 2017 *Phys. Rev. Lett.* **119** 023201
[10] Ferray M et al 1987 *J. Phys. B* **21** L31
[11] McPherson A et al 1987 *J. Opt. Soc. Am. B* **4** 595
[12] Winterfeldt C, Spielmann C and Gerber G 2008 *Rev. Mod. Phys.* **80** 117
[13] Parker J, Taylor K T and Clark C W 1996 *J. Phys. B* **29** L33
[14] Tong X-M and Chu S-I 1997 *Chem. Phys.* **217** 119
[15] Lein M, Gross E K U and Engel V 2000 *Phys. Rev. Lett.* **85** 4707
[16] Zielinski A, Majety V P and Scrinzi A 2016 *Phys. Rev. A* **93** 023406
[17] Paulus G G et al 1994 *J. Phys. B* **27** L703
[18] Panfili R, Haan S L and Eberly J H 2002 *Phys. Rev. Lett.* **89** 113001
[19] Corkum P B, Burnett N H and Brunel F 1989 *Phys. Rev. Lett.* **62** 1259
[20] Corkum P B 1993 *Phys. Rev. Lett.* **71** 1994
[21] Chen J et al 2000 *Phys. Rev. A* **63** 011404
[22] Keldysh L V 1965 *Soviet Physics - JETP* **20** 1307
[23] Faisal F H M 1973 *J. Phys. B* **6** L89
[24] Reiss H R 1980 *Phys. Rev. A* **22** 1786
[25] Popruzhenko S V 2014 *J. Phys. B* **47** 204001
[26] Milošević D B et al 2006 *J. Phys. B* **39** R203
[27] Wickenhauser M, Tong X M and Lin C D 2006 *Phys. Rev. A* **73** 011401
[28] Reiss H R and Krainov V P 1994 *Phys. Rev. A* **50** R910
[29] Arbó D G et al 2008 *Phys. Rev. A* **77** 013401
[30] Faisal F H M 2016 *Phys. Rev. A* **94** 031401
[31] Becker W, Lohr A and Kleber M 1994 *J. Phys. B* **27** L325
Lohr A et al 1997 *Phys. Rev. A* **55** R4003
Becker W et al 2002 *Adv. At. Mol. Opt. Phys.* **48** 35
[32] Smirnova O, Spanner M and Ivanov M 2006 *J. Phys. B* **39** S307
[33] Serebryannikov E E and Zheltikov A M 2016 *Phys. Rev. Lett.* **116** 123901
[34] Lewenstein M et al 1994 *Phys. Rev. A* **49** 2117
[35] Landau L D and Lifshitz E M 1977 *Quantum Mechanics* (Oxford: Pergamon)
[36] Gontier Y and Trahin M 1980 *J. Phys. B* **13** 4383
[37] Fabre F et al 1982 *J. Phys. B* **15** 1353
[38] Yudin G L and Ivanov M Y 2001 *Phys. Rev. A* **64** 013409
[39] Boge R et al 2013 *Phys. Rev. Lett.* **111** 103003
[40] Klaiber M, Hatsagortsyan K Z and Keitel C H 2015 *Phys. Rev. Lett.* **114** 083001
[41] Shvetsov-Shilovski N I et al 2016 *Phys. Rev. A* **94** 013415
[42] Li M et al 2014 *Phys. Rev. Lett.* **112** 113002
Geng J W et al 2015 *Phys. Rev. Lett.* **115** 193001
[43] Klaiber M and Briggs J S 2016 *Phys. Rev. A* **94** 053405
[44] Feit M D, Fleck J A Jr and Steiger A 1982 *J. Comput. Phys.* **47** 412
[45] Shirley J H 1965 *Phys. Rev.* **138** B979
[46] Delone N B and Kra V P 1999 *Phys.-Usp.* **42** 669